Effect of the order of He+ and H+ ion co-implantation on damage generation and thermal evolution of complexes, platelets, and blisters in silicon

Nabil Daghbouj, Nikolay Cherkashin, François-Xavier Darras, Vincent Paillard, M. Fnaiech, Alain Claverie

Effect of the order of He^+ and H^+ ion co-implantation on damage generation and thermal evolution of complexes, platelets, and blisters in silicon

N. Daghbouj, N. Cherkashin, F.-X. Darras, V. Paillard, M. Fnaiech, and A. Claverie

Citation: Journal of Applied Physics **119**, 135308 (2016); doi: 10.1063/1.4945032
View online: https://doi.org/10.1063/1.4945032
View Table of Contents: http://aip.scitation.org/toc/jap/119/13
Published by the American Institute of Physics

JOURNAL OF APPLIED PHYSICS **119**, 135308 (2016)

Effect of the order of He^+ and H^+ ion co-implantation on damage generation and thermal evolution of complexes, platelets, and blisters in silicon

N. Daghbouj,[1,2] N. Cherkashin,[1,a)] F.-X. Darras,[1] V. Paillard,[1] M. Fnaiech,[2] and A. Claverie[1]
[1]*CEMES-CNRS and Université de Toulouse, 29 rue J. Marvig, 31055 Toulouse, France*
[2]*Faculté des Sciences de Monastir, Université de Monastir, Monastir, Tunisia*

(Received 3 January 2016; accepted 18 March 2016; published online 7 April 2016)

Hydrogen and helium co-implantation is nowadays used to efficiently transfer thin Si layers and fabricate silicon on insulator wafers for the microelectronic industry. The synergy between the two implants which is reflected through the dramatic reduction of the total fluence needed to fracture silicon has been reported to be strongly influenced by the implantation order. Contradictory conclusions on the mechanisms involved in the formation and thermal evolution of defects and complexes have been drawn. In this work, we have experimentally studied in detail the characteristics of Si samples co-implanted with He and H, comparing the defects which are formed following each implantation and after annealing. We show that the second implant always ballistically destroys the stable defects and complexes formed after the first implant and that the redistribution of these point defects among new complexes drives the final difference observed in the samples after annealing. When H is implanted first, He precipitates in the form of nano-bubbles and agglomerates within H-related platelets and nano-cracks. When He is implanted first, the whole He fluence is ultimately used to pressurize H-related platelets which quickly evolve into micro-cracks and surface blisters. We provide detailed scenarios describing the atomic mechanisms involved during and after co-implantation and annealing which well-explain our results and the reasons for the apparent contradictions reported at the state of the art. © *2016 AIP Publishing LLC*.
[http://dx.doi.org/10.1063/1.4945032]

I. INTRODUCTION

High fluence hydrogen implantation was initially used in the Smart Cut™ technology to transfer thick silicon layers (i.e., >200 nm) onto another substrate.[1] Since then, it has been found that the co-implantation of H and He permits to substantially reduce the total fluence needed to fracture silicon[2–6] and thus the total cost of the SOI (Silicon On Insulator) wafers fabricated along this route. While the over-pressurization of H platelets by the He is generally admitted to be responsible for this "improvement," unfortunately, the physical phenomena involved and the mechanisms responsible for the effectiveness of the synergy between the two implants are still unclear, rendering this approach difficult to optimize and adapt to transfer thinner layers, as required for the fabrication of FDSOI (Fully Depleted SOI) wafers.

When implanting H only, the implanted hydrogen atoms and some of the vacancies generated by the implantation co-precipitate during annealing and form two-dimensional circular objects named platelets.[7,8] These platelets, filled with H_2 gas, grow in size during annealing until they become large enough and elastically interact and finally coalesce to form micro-cracks.[9] When these micro-cracks are close to the free surface of the wafer, the stress generated onto the silicon matrix by the pressure inside the platelets can elastically relax through the deformation of the surface, i.e., the formation of protuberances named blisters.[10] When this relaxation is prevented, for example, because a stiffener is intentionally rigidly bonded onto the wafer surface, the fracture of the whole implanted layer, parallel to the wafer surface, occurs during annealing. This is why, traditionally, the optimization of the fracture process is approached through the study of the blistering characteristics.

Summarizing the state of the art,[5,6,11–14] when co-implanting helium, it is generally thought that helium incorporates and over-pressurizes the hydrogen platelets during annealing and thus promotes their mechanical coalescence and the formation of blisters. It has been reported that this synergetic interaction was not so effective when He was implanted deeper than H and after H, likely because this second implant destroys the H related complexes formed after H implantation, while these complexes are thought to be the precursors of platelets and blisters.[5,6,11,12,14] Other authors proposed that the second implant leads to the amorphization of the damaged zone preventing the formation of Si-H internal surfaces and, thus, of platelets.[13] On the other hand, several researchers have apparently shown that the fracture of silicon is possible and even more effective when hydrogen is implanted first.[2,3,12]

In fact, all these works differ by the energies selected to implant the He and H ions. Depending on the case, the depth distribution of helium can be shallower than that of hydrogen,[12] can coincide more or less with it,[2,5] or can be located notably deeper.[2,4–6,10–16] Hence, these apparent influences of the order of implantation onto the effectiveness of the blistering or fracture phenomena might simply depend on whether or not the second specie travels through the entire profile of the first implanted one before immobilization.[12]

[a)]Author to whom correspondence should be addressed. Electronic mail: nikolay.cherkashin@cemes.fr.

The implanted fluences of He and H ions and the ratio between them have also an influence on the effectiveness of the fracture. For the ion energies commonly used in the industry and generally studied in the state of the art (i.e., 20–60 keV), the fracture is obtained for a minimum total fluence when shared in equal proportions between He and H (typically of 1×10^{16} ions/cm^2 for each implant). Any reduction of one of these two fluences must be compensated by a much larger increase of the other.[2,3,14] When lowering the ion implantation energies, the fracture can be obtained only by increasing significantly the H fluence, thus increasing the total fluence[6,17] needed to transfer a layer.

Implanting He and H in the unfavorable order has been noted to result in a considerable time delay (hours) of the blistering and splitting kinetics during low temperature annealing.[12,14] This has been tentatively interpreted as resulting from a larger incubation time for the nucleation of hydrogen platelets. However, this hypothesis was never proved, as the platelet populations were not characterized in detail. Since the destruction of the complexes, precursors of the platelets, is often invoked to explain the absence of platelets when He is implanted after having gone through the H profile,[5,6,11–14] one would expect the platelets to form when H goes through a shallower He profile. However, in that case also, splitting is not favored.[12] Finally, several authors, by assuming the H-related defects to be sole responsible for the differences observed in the blistering and splitting kinetics, have concluded that He out-diffuse from the implanted region when He, implanted in second, destroys the H-related complexes.[5,6] However, this scenario tends to ignore the probable interactions of He with the primary defects (I, V) and H-related complexes already feeding the silicon crystal.

For all these reasons, we have undertaken a systematic and detailed experimental study of the effect of the order of co-implantation, He then H (He-first) or H then He (H-first), on the formation of H and He related defects after implantation and on their evolution (transformation) during annealing at low and high temperatures.

We have chosen the respective H and He implantation energies so that the H and He concentration depth profiles partially superimpose, the He profile peak being located 50 nm deeper than the H one, when implanted alone. In a deliberate effort to master a process able to transfer thin layers suitable for the fabrication of FDSOI wafers, we have chosen to implant H and He at much lower energies than nowadays performed in the standard Smart Cut technology. The other conditions (concentrations and temperatures) are maintained as close as possible as those used in the standard process.

Using a variety of experimental techniques, we measure after each step the He and H depth distributions, the respective concentrations of the different hydrogenated complexes, the deformation profiles generated in the crystal by the defects, the types of defects, in relation to their sizes (from nanometers to micrometers) and, finally whether or not blistering is observed after annealing.

We then discuss our results and propose scenarios able to explain our experimental findings and those reported at the state of the art. These scenarios are built on a sequence of basic physical phenomena involving point defects, complexes, and extended defects and describe their evolutions from one type to the other. Finally, the effectiveness of the co-implantation synergy is elucidated and we establish the conditions for the optimization of the co-implantation technique.

II. EXPERIMENTAL DETAILS AND METHODOLOGY

(001) Si wafers covered by a 25 nm-thick thermally grown SiO_2 layer were implanted at room temperature with H only or co-implanted with H and He, H or He being implanted "first" (see Table I).

In general, the Smart Cut process is performed using energies in the 30–50 keV range.[2–4,9] In this work, we explore lower energies as they could be used to transfer thinner layers. The He^+ and H^+ implantation energies are such that He is implanted deeper than H while the fluences are such that the peak concentrations of both species are, after implantation, close to that used in the "conventional" Smart Cut technology. After implantation, the samples were eventually annealed either at 350 °C for 3 min or at 412 °C for 60 min under nitrogen gas in a conventional furnace.

The H and He depth distributions were measured by secondary ion mass spectroscopy (SIMS). The hydrogenated complexes found in the samples were identified via their signatures in the Raman spectra.[18] The out-of-plane strain profiles resulting from the implantation were obtained by simulating the X-ray (004) diffraction spectra obtained on the different samples and following the best fit procedure described in Refs. 19 and 20. Platelets, nano-bubbles, and micro-cracks were imaged using appropriate techniques of transmission electron microscopy (TEM).[8,21,22] The cavities buried in the implanted region of the samples were imaged by optical microscopy.[23] Finally, the blisters eventually appearing on the wafer surface were characterized by atomic force microscopy (AFM).[24,25]

III. EXPERIMENTAL RESULTS

A. H and He depth profiles

Figure 1 shows the H and He depth profiles measured by SIMS in the co-implanted samples (H first, Fig. 1(a); He first Fig. 1(b)). For comparison, the profiles simulated by the SRIM code,[26] which are proved to describe well the depth-profiles of H[20] and the He[27] provided that they were implanted alone, are also shown in the same figures.

Regardless of the order of co-implantation, the peaks of the H profiles measured by SIMS in the as-implanted samples are located slightly shallower than simulated by SRIM. While the H profile measured by SIMS in the He-first sample

TABLE I. Samples characteristics.

Sample	H-alone	H-first	He-first
First implant	H, 6 keV, 6×10^{15} H/cm^2	H, 6 keV, 6×10^{15} H/cm^2	He, 12 keV, 7×10^{15} He/cm^2
Second implant	No	He, 12 keV, 7×10^{15} He/cm^2	H, 6 keV, 6×10^{15} H/cm^2

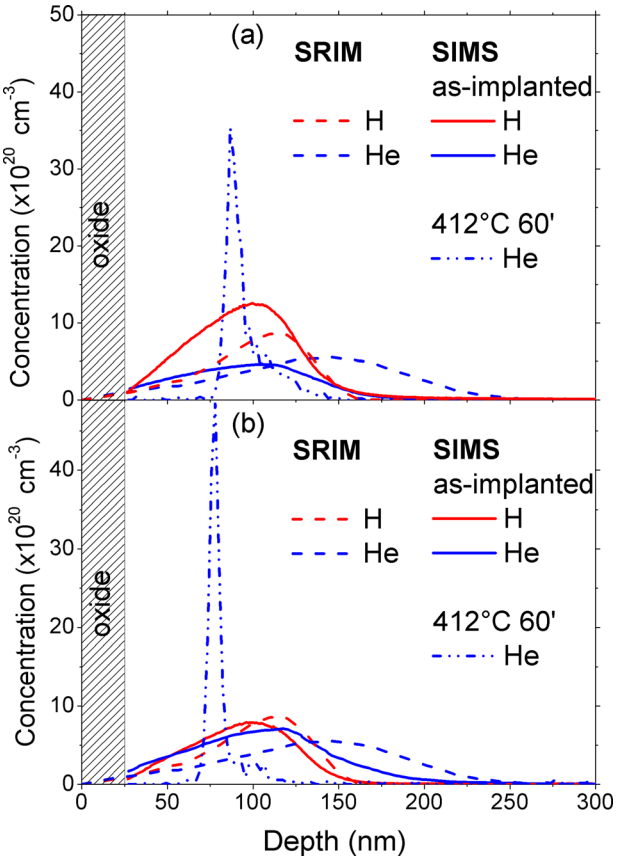

FIG. 1. H depth-distributions (red) and He depth-distributions (blue), measured by SIMS, after implantation (solid lines) or after annealing at 412 °C, 60 min (dashed-dotted line). The results of SRIM simulations are shown in dashed lines. (a) H-first and (b) He-first.

is quite similar to the one simulated by SRIM (Fig. 1(b)), the H fluence measured in the sample H-first seems to be 30% larger than expected (Fig. 1(a)).

The He profiles measured by SIMS in the two as-implanted samples are both much shallower than predicted by the simulations. While in the sample H-first the depth distribution of He measured by SIMS coincides quite well with the H profile (Fig. 1(a)), in the sample He-first, the experimental He profile extends slightly deeper than the H one (Fig. 1(b)). The measured He fluences of $5 \times 10^{15}\,\mathrm{cm}^{-2}$ for the sample H-first and of $7 \times 10^{15}\,\mathrm{cm}^{-2}$ for the sample He-first are close to the nominal values.

The comparison between the SRIM and the experimental profiles obtained for both orders of implantation shows that (i) the H depth distribution is not affected by He co-implantation, whatever its order, (ii) He, implanted deeper than H, always diffuses towards the H profile before annealing (i.e., at room temperature) and this, whatever the order of co-implantation, and (iii) this He trapping within the H profile is more pronounced in the sample H-first.

Whatever the order of implantation, annealing at 412 °C for 60 min gives rise to a dramatic redistribution of He and to its confinement within a thin (25 nm-thick) layer located at a depth of 80–90 nm from the surface of the wafer (Fig. 1, blue dashed-dotted lines). These profiles are asymmetric, abrupt at their upper interfaces while exhibiting tails towards the depth of the substrate. The measured He fluences of $5.2 \times 10^{15}\,\mathrm{cm}^{-2}$ for the sample H-first and of $4.6 \times 10^{15}\,\mathrm{cm}^{-2}$ for the sample He-first are close to the nominal values. The tail of the He profile is wider and contains a larger amount of He of $1.8 \times 10^{15}\,\mathrm{cm}^{-2}$ in the sample H-first than in the sample He-first which contains $0.9 \times 10^{15}\,\mathrm{cm}^{-2}$.

B. Out-of-plane strain profiles

Figure 2 shows the out-of-plane strain profiles we have extracted from our X-rays measurements.[28] Whatever the order of co-implantation, the out-of-plane strain is maximum at the depth where the H concentration is maximum. However, its amplitude depends on the order of co-implantation, being of 1.40% in the sample H-first (Fig. 2(a)) and of 0.73% in the sample He-first (Fig. 2(b)), both values being much larger than the 0.24% measured in the sample H-only (for a H concentration of $8 \times 10^{20}\,\mathrm{cm}^{-3}$).[20] Such differences demonstrate the dramatic contribution of He to the overall crystal deformation in the co-implanted samples, before annealing.

The shapes of the two profiles are also different. The strain profile obtained in the sample H-first is quasi-Gaussian, while the strain profile in the sample He-first has a deeper tail extending into the depth in the substrate. This shape characteristic is somehow similar to the one observed for the He depth distributions in the as-implanted samples (Fig. 1, solid line).

Annealing of the sample H-first only results in some weak narrowing of the strain profile (Fig. 2(a), solid line), its amplitude remaining unaffected. On the contrary, annealing of the sample He-first results in a strong narrowing of the profile (especially on its deeper side) and a dramatic increase of the maximum strain (Fig. 2(b), solid line). Again, this characteristic well reflects the redistribution of He which occurs during annealing (Fig. 1, dashed-dotted line).

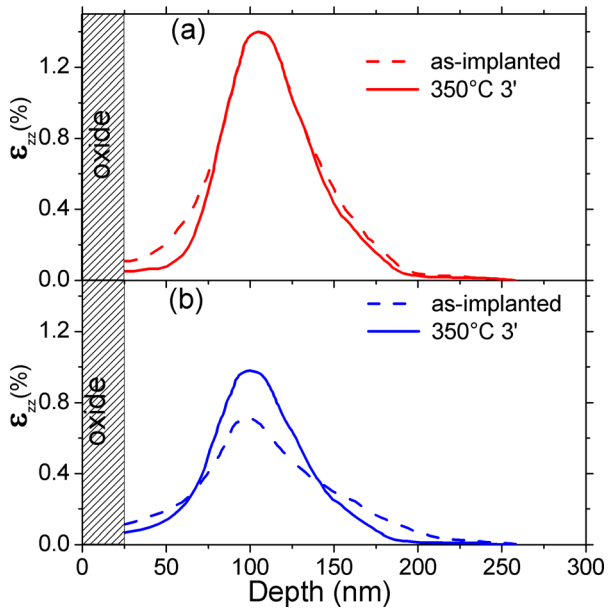

FIG. 2. Out-of- plane strain profiles in the as-implanted samples (dashed lines) and the samples annealed at 350 °C for 3 min (solid lines), co-implanted: (a) H-first and (b) He-first.

C. Hydrogenated complexes

Figure 3(a) shows the Raman spectra obtained from the samples implanted with H-alone (black line) and co-implanted, H-first (red line) and He-first (blue line), before annealing.

These spectra are quite different. The Raman spectrum obtained on the H-alone sample shows several characteristic signatures.[18,29] In the low frequency range (LF, $\lambda < 2050\,cm^{-1}$), these modes correspond to multi-vacancy hydrogenated complexes V_nH_m ($n \geq m$) and IH_2. In the high frequency range (HF, $\lambda > 2050\,cm^{-1}$), they correspond to the multi-hydrogen hydrogenated complexes such as VH_3,VH_4, and V_2H_6.

In the sample co-implanted H-first (red line), the spectrum intensity in the low frequency range is much higher than detected in the sample implanted with H alone. Conversely, the characteristic peaks assigned to the multi-hydrogen hydrogenated complexes (HF) are not detected.

In the sample co-implanted He-first (blue line), the spectrum intensity in the low frequency range is also higher than detected in the sample implanted with H alone, but it is lower than in the sample H-first. The signal corresponding to the V_2H_6 complex (HF range) shows about the same amplitude than in the sample implanted with H alone. The amplitude of the signal corresponding to the VH_4 complex is larger, that corresponding to the VH_3 complex is smaller, in this sample compared with what is observed in the H-alone sample.

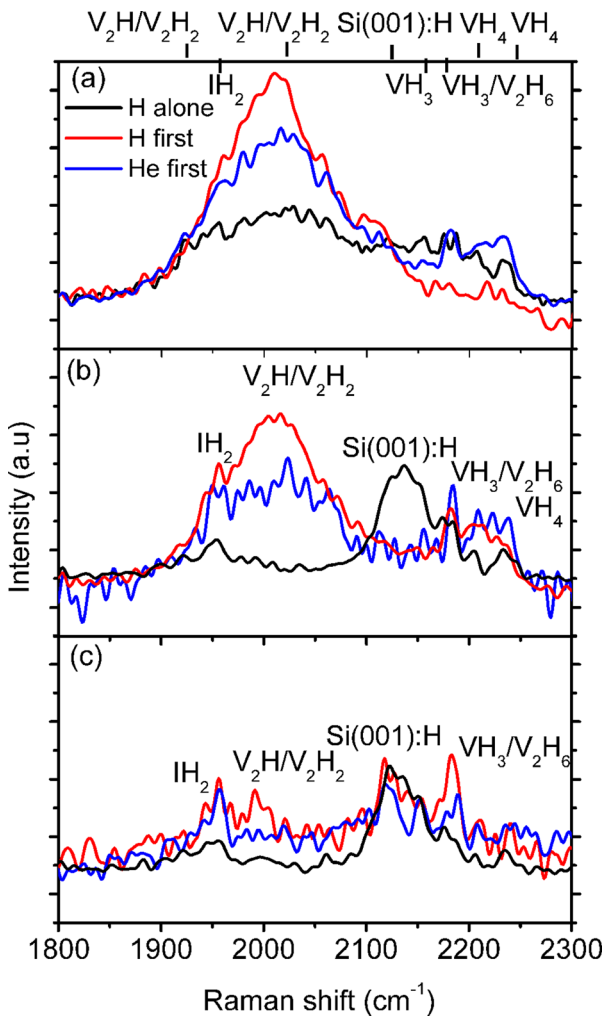

FIG. 3. Raman spectra obtained from the samples implanted with H alone (black line) and co-implanted H-first (red line) and He-first (blue line), before annealing.

The comparative analysis of the Raman spectra obtained from these three samples before annealing allows us to propose the following interpretation. After co-implantation and whatever its order, more hydrogen atoms contribute to the formation of multi-vacancy hydrogenated complexes and of the IH_2 complex than in the sample implanted with H alone. This shows that these complexes are formed preferably after co-implantation and thus take benefit from the additional damage provided by the second implant. The H fluence being the same in all these samples, the proportion of this fluence which contributes to the formation of multi-vacancy hydrogenated complexes and of the IH_2 complex depends on the amount of available damage, i.e., of Frenkel pairs, generated by the implantations. If our hypothesis is true, the resulting damage should be the largest after H-first co-implantation, smaller in the sample co-implanted He-first then the smallest in the sample implanted with H alone.

Figure 3(b) compares the Raman spectra obtained from the same samples after annealing at 350 °C for 3 min.

In the H-alone sample, annealing results in a strong decrease of the signals observed in the LF range and to the appearance of peaks in the HF range. The strong peak around $2125\,cm^{-1}$ is a characteristic of (001) Si-H passivated surfaces and conventionally assigned to the internal surfaces of objects such as hydrogen platelets and micro-cracks.[9] Higher frequency peaks are due to the multi-hydrogen hydrogenated complexes.

In the He-first sample, annealing results in a moderate decrease of the LF signals but the peaks in the HF range, associated to the multi-hydrogen hydrogenated complexes, already visible in the as-implanted state, remain the same after annealing. In contrast, in the H-first sample, the moderate decrease of the LF signals is compensated by appearance of the peaks associated to the multi-hydrogen hydrogenated complexes in the HF range.

Thus, while the spectra of the two co-implanted samples were different in the HF range before annealing, they are very similar after annealing. Still, the sample co-implanted H-first shows a much higher intensity in the LF range. These observations indicate that part of the multi-vacancy hydrogenated complexes and of the IH_2 complexes found after implantation and co-implantation dissociate during such an annealing. In the H-first sample, the VH_4 and the V_2H_6 complexes, which were not found after co-implantation, are formed during this annealing. This fact should be emphasized since the VH_4 or the V_2H_6 complexes are generally considered to be the precursors of platelets.[9]

Figure 3(c) compares the Raman spectra obtained in the same samples but after annealing at 412 °C for 60 min. Overall, these spectra are quite similar. By comparing the spectra obtained in the co-implanted samples with those shown after annealing at 350 °C for 3 min (Fig. 3(b)), we note that the signals corresponding to the multi-vacancy hydrogenated complexes and to the VH_4 complex have

disappeared, the peak corresponding to the V_2H_6 complexes stays unchanged, and that a new peak, characteristic of (001) surfaces passivated by hydrogen, has appeared. This shows that some complexes have been transformed into platelets and/or micro-cracks during this annealing.

Finally, we want to stress that while, before annealing, the populations of hydrogenated complexes are very different, in types and concentrations, depending on the order of co-implantation, these populations are less different after short time low temperature annealing and become almost similar after long time high temperature annealing.

D. Platelets, bubbles, and cracks

The observation of empty or gas-filled objects such as platelets and bubbles by TEM requires that images are taken far from dynamical Bragg conditions, to minimize strain contrast and out-of-focus to image the Fresnel fringes delimiting them.[7,8] Figure 4 shows a set of such (1–10) cross-sectional TEM images of the co-implanted samples after annealing.

First, we compare the samples annealed at 350 °C for 3 min (Figs. 4(a) and 4(b)). The sample H-first contains platelets of diameters less than 10 nm distributed over a 70 nm-thick band centered at a depth of 130 nm from the surface of the wafer (Fig. 4(a)). Their depth distribution corresponds to the H concentration profile shown in Fig. 1 and to the strain profile shown in Fig. 2 measured in this sample. Two families of platelets, {111} and {001}, coexist in this sample. The (001) variants (red arrows in the inset), parallel to the wafer surface, are distributed within the central part of the defect band, while the (11–1) and (111) variants are preferably located at the periphery of the defect band. Moreover, spherical bubbles with diameters of 1–3 nm are also detected (blue arrows in inset) in this sample. They are depth-distributed throughout the whole band containing the platelets.

In clear contrast, the sample He-first does not contain any bubbles. Only platelets, and/or nano-cracks, all parallel to the (001) surface of the wafer, of diameters ranging from 20 nm to 30 nm are found and are distributed within a 40 nm-thick band centered at the same 130 nm distance from the surface of the wafer (Fig. 4(b)). This depth-distribution is also similar to the H concentration profile (Fig. 1) and to the strain profile (Fig. 2) previously measured in this sample. However, while the average diameter of these platelets is larger than that found in the H-first sample, their density appears to be lower.

We now compare the samples annealed at 412 °C for 60 min. In the H-first sample (Fig. 4(c)), two types of objects, namely, nano-cracks (marked by green and red arrows in inset) and nano-bubbles (marked by blue arrows in inset), are detected. Nano-cracks predominantly parallel to the (001) surface of the wafer are confined within a 25–50 nm-thick band centered at a depth of about 125 nm from the wafer surface, i.e., where the H concentration is maximum. Few nano-cracks lie on the {111} planes (green arrow). Nano-bubbles of diameters in the 2–3 nm range are depth-distributed within a 100 nm-thick band centered at the same depth, but about three times thicker than the band containing the nano-cracks.

Again, the sample He-first does not contain any nano-bubbles after this annealing. Large micro-cracks, parallel to the (001) surface of the wafer, are observed (Fig. 4(d)). They are depth-distributed within a thin 25 nm-thick layer centered at a depth of 110 nm from the surface of the wafer.

Finally, after annealing, the main difference between the H-first and the He-first samples is that the He implanted fluence is totally and only incorporated into two-dimensional pressurized objects such as platelets, nano and micro-cracks in the He-first sample, while this same fluence is shared between such two-dimensional objects and nano-bubbles in the H-first samples.

E. Cavities and blisters

Figure 5 shows the plan view images obtained by optical microscopy and by AFM of the near surface of the co-implanted samples annealed at 412 °C for 60 min. The phase contrast in the optical micrographs arises from the

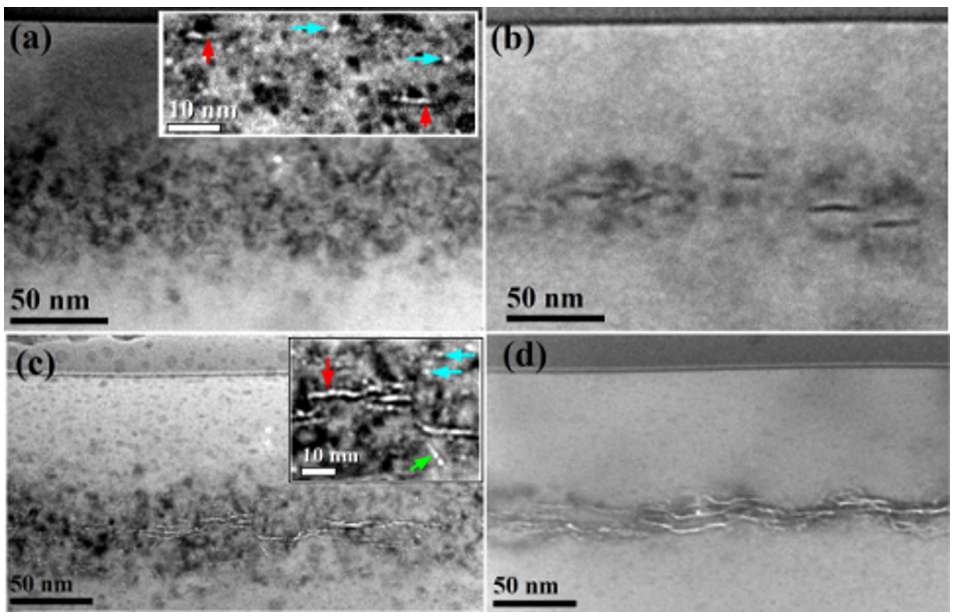

FIG. 4. (1–10) cross-sectional TEM images (Fresnel contrast) of the co-implanted and annealed samples: (a) and (c) Co-implanted H-first; (b) and (d) co-implanted He-first; (a) and (b) annealed 350 °C, 30 min; and (c) and (d) annealed 412 °C, 60 min. Insets in (a) and (c) show (001) and (111) platelets marked by red and green arrows, respectively, and He nano-bubbles marked by blue arrows.

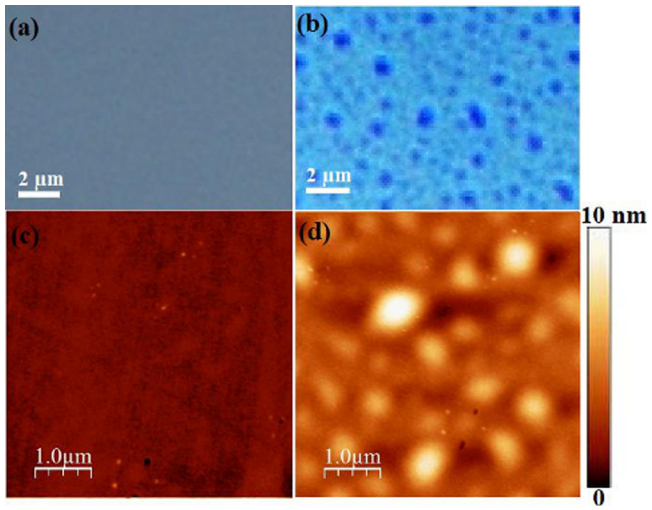

FIG. 5. Plan view images of the samples co-implanted then annealed at 412 °C for 60 min: (a) and (b) Optical micrographs; (c) and (d) AFM images; (a) and (c) H-first; and (b) and (d) He-first.

cavities buried at some depth in the crystal, while the AFM images reflect the morphology of the sample surfaces.[10]

Clearly, protuberances are seen on the surface of the sample co-implanted He-first (Fig. 5(d)), while not on the H-first sample (Fig. 5(c)). These blisters, of heights up to 10 nm, have an average diameter of 300 nm (varying from 200 nm to 1500 nm) and a density of 3.5 μm^{-2}. They occupy about 50% of the surface of the wafer. The optical image of Fig. 5(b) confirms the size and density characteristics of the cavities from which the blisters originate.[10]

IV. DISCUSSION

In this section, we discuss the "ingredients" and the mechanisms involved in the formation and thermal evolution of the defects found in silicon co-implanted by H and He as a function of the order of co-implantation. We will compare these mechanisms to those involved in the case where Si is implanted with H alone. From the experimental data presented in Section III, we can propose different scenarios to account for the similarities and the differences evidenced in the samples depending on the co-implantation order, from their as-implanted state to their annealed states, at low or high temperature.

Figure 6 shows schematically how the damage, i.e., the primary defects, interstitials (I), vacancies (V), and H atoms, is "shared" and combined to form the I_n, the V_n, and the different hydrogenated complexes, after H-alone implantation (first column), H-first co-implantation (second column), and He-first co-implantation (third column). The different lines represent the different successive steps of implantation and "precipitation" occurring at room temperature, depending on the samples. The last line describes the situation after annealing.

It is known that a variation of any of the concentrations of Is and Vs formed by implantation affects the repartition of H and of these defects between the different types of complexes which can be formed at room temperature.[18,20,23] We have evidenced this fact through Raman spectroscopy: after co-implantation in any order, a larger part of the H fluence

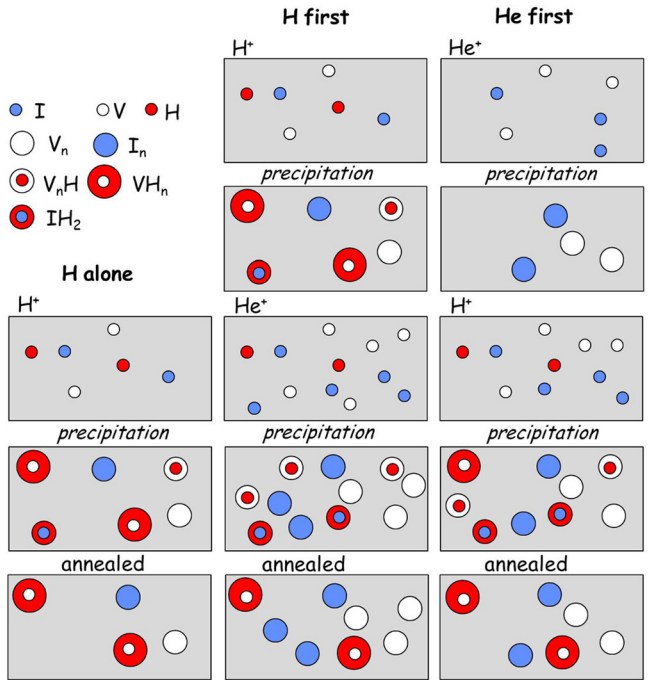

FIG. 6. Evolution of the damage constituents after H alone implantation (first column), H-first co-implantation (second column), and He-first co-implantation (third column). The various complexes which form are represented by symbols. When the same symbol is used several times, it indicates a larger density of the complex.

contributes to the formation of multi-vacancy hydrogenated complexes and of the IH_2 complexes than observed in the case of a H-alone implantation (Fig. 6, fourth line). The efficiency of this synergetic effect between primary defects and hydrogen does depend on the order of co-implantation. Indeed, the second implantation destroys the complexes formed after the first implantation (Fig. 6, second line), as evidenced in Fig. 3(a). This ballistic dissociation results in the injection of "extra" interstitials and vacancies in addition to those generated by that second implantation itself (Fig. 6, third line). We know that the damage generated by He implantation is typically three to four times higher than that generated by H implantation.[26] Therefore, H being implanted at a smaller depth, a much larger number of interstitials and vacancies are generated when He passes through the H profile. Hence, when He is implanted after H, it is more probable to form multi-vacancy hydrogenated complexes and IH_2 complexes than multi-hydrogen hydrogenated complexes. This is depicted in Fig. 6.

We also know that He implantation results in the formation of nano-bubbles, i.e., co-precipitates of He and vacancies, and this at room temperature.[7,21] It is therefore very likely that when implanting He first, we promote the trapping of He within the vacancy-rich complexes, what is coherent with the thermal redistribution of He within the H profile that we have observed by SIMS (Fig. 1). Moreover, part of the H fluence participates in the formation of multi-hydrogen hydrogenated complexes, the precursors of platelets, which immediately offer efficient trapping sites to the He atoms. Conversely, when H is implanted first, the multi-hydrogen hydrogenated complexes are not formed (Fig. 3(a)). Thus,

He can agglomerate only within the nano-bubbles and/or contribute to the formation of the multi-vacancy hydrogenated complexes (Fig. 6, fourth line).

During annealing, the less stable complexes decompose and/or transform into complexes or precipitates more stable at the considered temperature.[18] When H is implanted alone, the multi-vacancy hydrogenated complexes and the IH_2 complexes are relatively unstable compared with the VH_4 and the V_2H_6 complexes.[20] They thus dissolve during annealing[18] (Fig. 6, last line). Personnic *et al.*[9] have shown that the VH_4 and the V_2H_6 complexes are quite stable and continuously evolve and transform into platelets during annealing. Thus, these complexes can be formed again at the beginning of some annealing (as observed by Raman spectroscopy and shown in Fig. 3(b)), evolve during annealing until also, and finally contributing to the formation of platelets (Fig. 3(c)).

However, the amount of He atoms available after co-implantation for being trapped within platelets during annealing depends on their initial distribution between the complexes found before annealing. When He gets incorporated within the multi-vacancy hydrogenated complexes during annealing, these complexes do not dissolve but preferably transform into nano-bubbles filled with He. Indeed, after He-alone ion implantation, these nano-bubbles, once they are formed, are very stable even surviving high temperature annealing and may coexist with platelets.[7,30–32] Thus, after H-first co-implantation and before annealing, He atoms are massively incorporated within the multi-vacancy hydrogenated complexes and also within the pure vacancy complexes (V_n in Fig. 6). During annealing, they agglomerate in the form of nano-bubbles. For this reason, after annealing, the hydrogen platelets seen after H-first co-implantation contain less He than those formed after co-implantation with He first. As a result, platelets formed after H-first co-implantation and annealing are less pressurized than those formed after He-first co-implantation and annealing. This characteristic is confirmed by the observation that the platelets found in the He-first sample after annealing are only of the (001) type, i.e., parallel to the wafer surface, while they can be of the (111) family, i.e., inclined with respect to the surface plane in the H-first co-implanted sample.[21,33] Being less pressurized and not always aligned with the wafer surface, their mechanical coalescence leading to the formation of micro-cracks is less efficient. Hence, the system evolves differently during annealing depending on how He was initially distributed before annealing, within the nano-bubbles and/or various hydrogenated complexes. This is why, and not because of the effusion of He and H_2, as proposed in Refs. 5 and 6, that blistering may be not observed after annealing of H-first co-implanted silicon, while it can be observed, for the same implantation conditions, by reversing the order of the co-implantation.

V. CONCLUSIONS

In this work, we have studied, using a very large variety of experimental techniques, the mechanisms involved in the formation and thermal evolution of defects and complexes formed in silicon after H and He co-implantation, specifically focusing on the influence of the implantation order on this evolution. We have compared these defects and their evolutions with those obtained in the case of implantation of H alone. The implantation energies were chosen in order to partially superimpose the H and the He profiles, the He profile being deeper than the H one.

We have confirmed that the order of co-implantation has a dramatic influence on the final results of annealing, i.e., blistering or no blistering. We have demonstrated that this difference arises from a difference in the concentrations of interstitials and vacancies available before annealing which in turn affects the distributions of H and He within the various defects and complexes which are formed after implantation, then after annealing.

Specifically, the implantation of the second species tends to destroy the complexes already formed after the first implantation. The elementary constituents provided by these complexes are added to the primary defects generated by the second implantation. All of them become available for the formation of new complexes. Since He ions are heavier than H ions and generate defects in the whole region where H is implanted, the post-implantation of He provides the system with a larger amount of primary defects than when implanting He-first and, much more than when H is implanted alone.

These differences finally derive the relative distributions of H and He between the different complexes that can be formed in the region where H is available, after implantation and after annealing.

When H is implanted alone, the H atoms are distributed between the multi-hydrogen hydrogenated complexes, the multi-vacancy hydrogenated complexes, and the IH_2 complexes. The co-implantation of He and H changes the proportions between these various complexes. In particular, when He is implanted through the H profile (H-first co-implantation), the concentration of available primary defects is the largest and the multi-hydrogen hydrogenated complexes are not formed.

The higher the concentration of multi-vacancy hydrogenated complexes and the larger the generated damage are, the more easily and effectively He atoms are trapped at the depth where H is present. During annealing, the multi-vacancy hydrogenated complexes transform into He nano-bubbles, while the multi-hydrogen hydrogenated complexes transform into platelets pressurized by a mixture of He and H_2 gases. Hence, the system evolves differently during annealing depending on how He was initially distributed, before annealing, within the nano-bubbles and and/or various hydrogenated complexes. After H-first co-implantation and during short time annealing, the multi-hydrogen hydrogenated complexes, initially destroyed by the second implant, are rapidly reformed finally contributing to the formation of platelets. After long time annealing, the system evolves until forming nano-cracks and nano-bubbles which host the whole fluence of implanted He, without forming micro-cracks nor blisters. In contrast, when He is implanted first, the platelets have no competitor to store He atoms: they are thus more pressurized and their easier mechanical coalescence leads to the formation of micro-cracks and cavities and finally blisters through the elastic deformation of the surface.

[1]M. Bruel, Electron. Lett. **31**, 1201–1202 (1995).
[2]P. Nguyen, I. Cayrefourcq, K. K. Bourdelle, A. Boussagol, E. Guiot, N. Ben Mohamed, N. Sousbie, and T. Akatsu, J. Appl. Phys. **97**, 083527 (2005).
[3]A. Agarwal, T. E. Haynes, V. C. Venezia, O. W. Holland, and D. J. Eaglesham, Appl. Phys. Lett. **72**(9), 1086 (1998).
[4]S. Reboh, A. A. de Mattos, J. F. Barbot, A. Declemy, M. F. Beaufort, R. M. Papaléo, C. P. Bergmann, and P. F. P. Fichtner, J. Appl. Phys. **105**, 093528 (2009).
[5]O. Moutanabbir, B. Terreault, M. Chicoine, F. Schiettekatte, and P. J. Simpson, Phys. Rev. B **75**, 075201 (2007).
[6]O. Moutanabbir and B. Terreault, Appl. Phys. Lett. **86**, 051906 (2005).
[7]N. Cherkashin and A. Claverie, "TEM in micro-nanoelectronics," in *Characterization of Process-Induced Defects*, edited by A. Claverie (WILEY, 2012), pp. 165–193, ISBN: 9781848213678.
[8]J. Grisolia, G. Ben Assayag, A. Claverie, B. Aspar, C. Lagahe, and L. Laanab, Appl. Phys. Lett. **76**, 852 (2000).
[9]S. Personnic, K. K. Bourdelle, F. Letertre, A. Tauzin, N. Cherkashin, A. Claverie, R. Fortunier, and H. Klocker, J. Appl. Phys. **103**, 023508 (2008).
[10]N. Cherkashin, N. Daghbouj, F.-X. Darras, M. Fnaiech, and A. Claverie, J. Appl. Phys. **118**, 245301 (2015).
[11]C. Qian, B. Terreault, and S. C. Gujrathi, Nucl. Instrum. Methods Phys. Res., Sect. B **175–177**, 711–714 (2001).
[12]C. Lagahe-Blanchard, N. Sousbie, S. Sartori, H. Moriceau, A. Sousbie, B. Aspar, P. Nguyen, and B. Blondeau, Proc. Electrochem. Soc. **19**, 346 (2003).
[13]P. Nguyen, K. K. Bourdelle, T. Maurice, N. Sousbie, A. Boussagol, X. Hebras, L. Portigliatti, F. Letertre, A. Tauzin, and N. Rochat, J. Appl. Phys. **101**, 033506 (2007).
[14]J. H. Liang, H. Y. Hsieh, C. W. Wu, and C. M. Lin, Nucl. Instrum. Method Phys. Res., Sect. B **365**(A), 128–132 (2015).
[15]M. K. Weldon, M. Collot, Y. J. Chabal, V. C. Venezia, A. Agarwal, T. E. Haynes, D. J. Eaglesham, S. B. Christman, and E. E. Chaban, Appl. Phys. Lett. **73**(25), 3721 (1998).
[16]X. Duo, W. Liu, M. Zhang, L. Wang, C. Lin, M. Okuyama, M. Noda, W.-Y. Cheung, S. P. Wong, P. K. Chu, P. Hu, S. X. Wang, and L. M. Wang, J. Appl. Phys. **90**(8), 3780 (2001).
[17]C. Qian and B. Terreault, J. Appl. Phys. **90**, 5152 (2001).
[18]O. Moutanabbir and B. Terreault, J. Chem. Phys. **121**, 7973 (2004).
[19]N. Sousbie, L. Capello, J. Eymery, F. Rieutord, and C. Lagahe, J. Appl. Phys. **99**, 103509 (2006).
[20]N. Cherkashin, F.-X. Darras, P. Pochet, S. Reboh, N. Ratel-Ramond, and A. Claverie, Acta Mater. **99**, 187–195 (2015).
[21]X. Hebras, P. Nguyen, K. K. Bourdelle, F. Letertre, N. Cherkashin, and A. Claverie, Nucl. Instrum. Methods Phys. Res., Sect. B **262**, 24 (2007).
[22]J. Grisolia, F. Cristiano, G. Ben Assayag, and A. Claverie, Nucl. Instrum. Methods Phys. Res., Sect. B **178**, 160 (2001).
[23]J.-D. Penot, D. Massy, F. Rieutord, F. Mazen, S. Reboh, F. Madeira, L. Capello, D. Landru, and O. Kononchuk, J. Appl. Phys. **114**, 123513 (2013).
[24]O. Moutanabbir, A. Giguére, and B. Terreault, Appl. Phys. Lett. **84**, 3286 (2004).
[25]R. Singh, S. H. Christiansen, O. Moutanabbir, and U. Gösele, J. Electron. Mater. **39**, 2177 (2010).
[26]J. F. Ziegler and J. P. Biersack, SRIM computer code, see http://www.srim.org.
[27]M. Vallet, J. F. Barbot, A. Declémy, S. Reboh, and M. F. Beaufort, J. Appl. Phys. **114**, 193501 (2013).
[28]S. A. Stepanov, 2007, see http://sergey.gmca.aps.anl.gov/gid_sl.html.
[29]O. Moutanabbir, B. Terreault, M. Chicoine, and F. Schiettekatte, Appl. Phys. A **80**, 1455–1462 (2005).
[30]F. Corni, C. Nobili, G. Ottaviani, R. Tonini, G. Calzolari, G. F. Cerofolini, and G. Queirolo, Phys. Rev. B **56**(12), 7331 (1997).
[31]M.-L. David, K. Alix, F. Pailloux, V. Mauchamp, M. Couillard, G. A. Botton, and L. Pizzagalli, J. Appl. Phys. **115**, 123508 (2014).
[32]S. Fréchard, M. Walls, M. Kociak, J. P. Chevalier, J. Henry, and D. Gorse, J. Nucl. Mater. **393**(1), 102 (2009).
[33]N. Cherkashin, F. X. Darras, and A. Claverie, Solid State Phenom. **242**, 190–195 (2015).